Comments on Inorganic Chemistry
Publication details, including instructions for authors and subscription information:
http://www.informaworld.com/smpp/title~content=t713455155

Unusual Features in Absorption Spectra Arising from Coupled Potential Surfaces

Christian Reber[a]; Jeffrey I. Zink[b]
[a] Department of Chemistry, University of Montreal, Montreal, Quebec, Canada [b] Department of Chemistry and Biochemistry, University of California, Los Angeles, California

To cite this Article Reber, Christian and Zink, Jeffrey I.(1992) 'Unusual Features in Absorption Spectra Arising from Coupled Potential Surfaces', Comments on Inorganic Chemistry, 13: 3, 177 — 220
To link to this Article: DOI: 10.1080/02603599208052195
URL: http://dx.doi.org/10.1080/02603599208052195

Unusual Features in Absorption Spectra Arising from Coupled Potential Surfaces

CHRISTIAN REBER
Department of Chemistry,
University of Montreal,
Montreal (Quebec) H3C 3J7,
Canada

JEFFREY I. ZINK
Department of Chemistry and Biochemistry,
University of California,
Los Angeles, California 90024

Received January 30, 1992

The purpose of this Comment is to introduce the calculation and interpretation of unusual features in absorption spectra arising from coupled potential surfaces by using time dependent theory. A wide variety of spectroscopic phenomena are examined and spectra are calculated with new time dependent quantum mechanical methods. Examples include intensity borrowing, vibronic structure in intraconfigurational d-d transitions, interference dips on broad, unresolved absorption bands, the Jahn–Teller effect in the final state of an absorption transition and the intervalence absorption band. Comparisons of the theoretical calculations with experimental spectra are given and the potential for future applications is discussed.

Key Words: *absorption spectra, band shapes, potential surfaces, coupled potentials*

1. INTRODUCTION

What are the new and interesting areas of research in the field of electronic absorption spectroscopy of transition metal compounds?

Comments Inorg. Chem.
1992, Vol. 13, Nos. 3 & 4, pp. 177–220
Reprints available directly from the publisher
Photocopying permitted by license only

Aren't band shapes, widths and vibronic structure understood in terms of Franck–Condon factors? Aren't the transition energies understood in terms of ligand field theory or molecular orbital theory? Certainly the most general answer to the latter two questions is a reserved "yes"; the overall spectroscopic features of many metal compounds, especially classical "Werner" complexes, are quite well understood. But detailed examination of electronic spectra continue to reveal surprising features that cannot be simply explained by the ordinary elements of the commonly applied theories. The spectra of metal compounds are very rich. Many different types of transitions occur closely spaced in energy, and most of the excited states have structures different from that of the ground electronic state resulting in spectra containing vibronic progressions from many normal modes.[1] One source of surprising spectroscopic features is coupling between electronic states. The interpretation and calculation of the spectroscopic effects of coupling by using time dependent theory is a new and interesting area of research. An introduction to this research forms the basis of this Comment.

Most spectroscopic interpretations are based on a picture in which the nuclei are clamped in the ground state equilibrium position. This picture implies the Born–Oppenheimer approximation where the electronic and nuclear wavefunctions are separable.[2] In this picture, the electronic states line up like rungs on a ladder, each with a specific energy. The total absorption spectrum is the sum of transitions to each rung. If a transition to a given rung is forbidden (e.g., by spin selection rules), a perturbation (e.g., spin-orbit coupling) mixes in part of an allowed rung, changes the energy slightly, and causes the transition to become allowed.

But what about nuclear motions? As the nuclei move, the energies of the electronic states can change. The plot of the energy as a function of the nuclear position defines a diabatic potential surface. The electronic energies can change their relative positions, i.e., a high and a low energy rung can switch positions and at some value of the nuclear positions the plots cross. However, ignoring the coupling between the nuclear and electronic wavefunctions can lead to erroneous results. For example, two rungs of the ladder might be calculated to have the same energy and be degenerate when nuclear motion is ignored, a situation which is impossible

according to the Jahn–Teller theorem.[3] An interpretation of the spectrum based on the Born–Oppenheimer approximation would also be in error in this case.

The most obvious spectroscopic manifestation of a change in the nuclear positions between the ground and excited electronic states is vibronic structure (or broad absorption bands if the individual vibronic components are not resolved). If we operate in the picture where the nuclear wavefunction is separable from the electronic wavefunction, then the usual treatment of the vibronic part of the problem is a Franck–Condon analysis. The transition to each rung on the ladder then consists of vibronic progressions starting from the electronic origin. Many interesting situations do not allow separability. As mentioned above, the Jahn–Teller effect is one example. Another example which we will extensively discuss is crossing diabatic surfaces that are coupled. The latter leads to spectroscopic features which at first glance appear mysterious such as dips or losses of intensity in broad absorption envelopes.

The unifying feature of this Comment is the calculation and interpretation of electronic spectra in terms of two diabatic potential surfaces along a non-degenerate normal coordinate. All of the spectra will be calculated by using either a symmetric disposition of the surfaces as shown in Fig. 1a or an asymmetric disposition as shown in Fig. 1b. Both the diabatic and adiabatic potential surfaces are shown in Fig. 1. In both Figs. 1a and 1b the

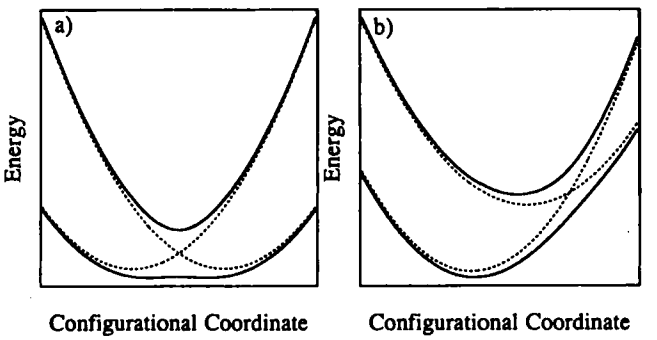

FIGURE 1 Coupled potential energy surfaces. Diabatic and adiabatic surfaces are shown as dotted and solid lines, respectively. (a) Symmetric disposition, (b) asymmetric disposition.

diabatic surfaces cross and the clamped nuclei picture is erroneous. The symmetric arrangement is rather special, but not uncommon in the spectroscopy of highly symmetrical metal complexes. It will be used to treat both the Jahn–Teller coupling problem and the intervalence electron transfer problem. We use the asymmetric case to treat details of intensity borrowing by spin-orbit coupling. In addition, it is used to calculate and explain interference dips in absorption envelopes. These examples show that electronic spectra are not the simple superposition of absorption bands to rungs on a ladder!

We begin our Comment with a description of the theoretical tools. New time dependent theoretical methods make it easy to calculate and interpret electronic spectra in terms of coupled potential surfaces, providing exact quantum mechanical results as well as a new viewpoint and new insight. We apply these tools to a variety of spectroscopic problems. Our first example is intensity borrowing by spin-orbit coupling. We use the asymmetric arrangement of surfaces where the transition to one of the diabatic surfaces is spin-forbidden. Integrated band intensities are calculated. Second, we use a similar example to calculate the resolved vibronic structure in spin-forbidden transitions. The structure is not simply that expected from the "forbidden" state with non-zero intensity. Third, we show that surface coupling leads to interference between two states and that the resulting spectrum is far from the sum of the spectra from the two states individually. Our final two examples use the symmetric arrangement of potential surfaces. We calculate absorption spectra for transitions from a non-degenerate ground state into a Jahn–Teller coupled excited state. We also calculate transitions within the coupled surfaces which represent intervalence electron transfer bands.

2. THEORETICAL METHOD

In this section we briefly present the theoretical foundation underlying the calculation of the transition metal spectra shown in the following sections. We focus on the treatment of coupled excited state potential surfaces in the framework of the time dependent theory of molecular spectroscopy. The time dependent approach

is very powerful from both the technical and conceptual points of view. This is particularly evident in the treatment of coupled electronic states: in the time independent (Franck–Condon) picture, the spectroscopic consequences of coupling between states are much harder to qualitatively visualize and to quantitatively calculate than with time dependent methods.

The fundamental equation for the calculation of an absorption spectrum in the time dependent theory is[4,5]:

$$I(\omega) = C\omega \int_{-\infty}^{+\infty} \exp(i\omega t) \cdot \left\{ \langle \phi | \phi(t) \rangle \exp\left(-\Gamma^2 t^2 + \frac{iE_0}{\hbar} t \right) \right\} dt \quad (1)$$

with $I(\omega)$ the absorption intensity at frequency ω, E_0 the energy of the electronic origin transition and Γ a phenomenological Gaussian damping factor. The most important ingredient to Eq. (1) is $\langle \phi | \phi(t) \rangle$, the autocorrelation function of the wavepacket ϕ prepared on an excited state potential surface after the spectroscopic transition. The wavepacket $\phi(t)$ is evolving on this surface with time. For two coupled excited states, the situation which we examine in this Comment, we need to keep track of two wavepackets, ϕ_1 and ϕ_2 moving on the two coupled potential surfaces.[6–11] The total overlap $\langle \phi | \phi(t) \rangle$ is calculated as:

$$\langle \phi | \phi(t) \rangle = \langle \phi_1 | \phi_1(t) \rangle + \langle \phi_2 | \phi_2(t) \rangle. \quad (2)$$

The initial wavepackets are:

$$\phi_i = \phi_i(t = 0) = \mu_i \chi(Q) \quad (i = 1,2) \quad (3)$$

with μ_i^2 the electronic transition moment for an absorption to excited state i and $\chi(Q)$ the thermally weighted sum of all populated ground state levels. We confine ourselves to situations where only the lowest ground state level is populated, a situation that applies to low temperature absorption spectroscopy. For simplic-

ity, we assume a harmonic ground state potential in all the examples presented here, with the exception of the intervalence absorption bands calculated in Section 3.5. The wavefunctions ϕ_i at $t = 0$ are therefore Gaussians. This is not a fundamental limitation of the theory; the absolute overlap $\langle\phi|\phi(t)\rangle$ can be calculated for any given initial function. For simplicity, the transition moments μ_i were chosen to be coordinate independent, i.e., constants, in all the following examples.

For the calculation of the autocorrelation function in Eq. (1) we need $\phi_i(t)$, the propagating wavefunction in the two coupled potential surfaces. It is given by the time dependent Schrödinger equation, written here for one state i in dimensionless form[12]:

$$i\frac{\partial\phi_i}{\partial t} = -\frac{1}{2M}\nabla^2\phi_i + V_i(Q)\phi_i = H_i\phi_i \tag{4}$$

where H_i denotes the Hamiltonian, $V_i(Q)$ is the potential energy as a function of the configurational coordinate Q and $-1/2M\cdot\nabla^2$ the nuclear kinetic energy. For simplicity we choose harmonic excited state potentials in all the following examples, although the theoretical method is not restricted by the functional form of the potentials. The potentials are given by:

$$V_i(Q) = \frac{1}{2}k_i(Q - \Delta Q_i)^2 + E_i \tag{5}$$

with $k_i = 4\pi^2M(\hbar\omega_i)^2$ the force constant, ΔQ_i the position of the potential minimum along Q and E_i the energy of the potential minimum for state i. These uncoupled potentials are shown as dashed lines in Fig. 1 (diabatic potentials). The coupling between the diabatic potentials for states 1 and 2 is chosen to be coordinate independent in this Comment:

$$V_{12} = V_{21} = \text{const.} \tag{6}$$

Again, the computational method allows us to use coordinate dependent coupling. The most important coupling mechanism in transition metal spectra is spin-orbit coupling which does not strongly

depend on nuclear coordinates and makes Eq. (6) a good approximation. The time dependent Schrödinger equation for two coupled states is given by:

$$i\frac{\partial \phi_i}{\partial t} = \begin{pmatrix} H_1 & V_{12} \\ V_{21} & H_2 \end{pmatrix} \begin{pmatrix} \phi_1 \\ \phi_2 \end{pmatrix} \tag{7}$$

with the diagonal elements H_i of the total Hamiltonian as given in Eq. (4).

In order to calculate $\phi_i(t)$ we use the split operator method developed by Feit and Fleck.[12-14] Both the configurational coordinate Q and the time are represented by a grid with points separated by ΔQ and Δt, respectively. For one surface, the time dependent wavefunction $\phi(Q,t + \Delta t)$ is obtained from $\phi(Q,t)$ with:

$$\begin{aligned} \phi(t + \Delta t) = \exp\left(\left(\frac{i\Delta t}{4M}\right)\nabla^2\right) \exp(-i\Delta t V) \\ \exp\left(\left(\frac{i\Delta t}{4M}\right)\nabla^2\right) \phi(Q,t) + O[(\Delta t)^3] \\ = \hat{P}\hat{V}\hat{P}\phi(Q,t) + O[(\Delta t)^3]. \end{aligned} \tag{8}$$

This equation is generalized to the case of two coupled potentials as follows. The exponential operators $\hat{P}$ and $\hat{V}$ in Eq. (8) are replaced by 2×2 matrices operating simultaneously on $\phi_1(Q,t)$ and $\phi_2(Q,t)$:

$$\begin{pmatrix} \phi_1(Q,t + \Delta t) \\ \phi_2(Q,t + \Delta t) \end{pmatrix}$$

$$= \begin{pmatrix} \hat{P}_1 & 0 \\ 0 & \hat{P}_2 \end{pmatrix} \begin{pmatrix} \hat{V}_1 & \hat{V}_{12} \\ \hat{V}_{21} & \hat{V}_2 \end{pmatrix} \begin{pmatrix} \hat{P}_1 & 0 \\ 0 & \hat{P}_2 \end{pmatrix} \begin{pmatrix} \phi_1(Q,t) \\ \phi_2(Q,t) \end{pmatrix} + O[(\Delta t)^3]. \tag{9}$$

The kinetic energy operator $\hat{P}$ is independent for ϕ_1 and ϕ_2 in the diabatic basis, i.e., its matrix is diagonal. The potential energy

operator $\hat{V}$ is more intricate. The exponential operators must be given in terms of potentials that diagonalize the potential matrix in the total Hamiltonian, Eq. (7), i.e., in terms of the adiabatic potentials V_a and V_b. These potentials are calculated from the diabatic potentials V_1 and V_2 and the coupling V_{12}:

$$V_a = c_1 V_1 + c_2 V_2$$

$$= \frac{1}{2}\{(V_1 + V_2) - \sqrt{(V_1 - V_2)^2 + 4V_{12}}\}, \quad (10)$$

$$V_b = c_2 V_1 - c_1 V_2$$

$$= \frac{1}{2}\{(V_1 + V_2) + \sqrt{(V_1 - V_2)^2 + 4V_{12}}\}. \quad (11)$$

From Eq. (9) it is obvious that $\phi_1(t)$ and $\phi_2(t)$ are mixed (formally via the off-diagonal matrix elements $\hat{V}_{12}$) at each time step. Details of the computer implementation of Eq. (9) are given in the literature.[6-11] The method is not computer time intensive: a typical calculation as presented in this Comment takes on the order of 10 s CPU time on a Silicon Graphics 4D/380 computer. The CPU time is determined by the speed of the fast Fourier transform algorithm. We use a routine from the literature in all our calculations, in order to be as independent as possible from specific computers or subroutine libraries.[15]

It is interesting to note the different roles of $\hat{P}$ and $\hat{V}$. $\hat{P}$, the momentum operator, transfers wavefunction amplitude ϕ_i among grid points along Q at each time step, but does not transfer amplitude between the diabatic parent states 1 and 2. These changes are easily monitored by looking at the wavepacket $\phi_i(t)$ after every time step. On the other hand, $\hat{V}$, the potential energy operator, transfers amplitude between the electronic states at each time step, but does not couple grid points along Q. The amplitude transfer between the diabatic potentials can be followed by calculating the norms $\langle\phi_i(t)|\phi_i(t)\rangle$ for $\phi_1(t)$ and $\phi_2(t)$ after every time step. The norms are a quantitative measurement for the amount of popu-

lation change between the two states, as illustrated in the following section.

Both operators affect the total overlap $\langle\phi|\phi(t)\rangle$ in Eq. (1) and therefore the absorption spectrum. Only the calculation which simultaneously involves both coupled states according to Eq. (9) gives the correct total overlap. All calculations involving only one surface lack the contribution of the population change between the states to the total dynamics due to nonadiabatic transitions or "surface hopping." In the time dependent picture it is straightforward to see how these population changes, direct manifestations of the breakdown of the Born–Oppenheimer approximation, occur and what their influences on the absorption spectrum are.

Experimental absorption spectra often show progressions in many normal modes. In the framework of time dependent theory it is easy to calculate a spectrum involving several normal coordinates by using a series of one-dimensional propagations. In the absence of coupling terms between the normal coordinates, the total autocorrelation in a system with k coordinates is given by:

$$\langle\phi|\phi(t)\rangle = \prod_k \langle\phi_k|\phi_k(t)\rangle. \tag{12}$$

In this Comment only one-dimensional potential surfaces will be examined, but for the quantitative interpretation of an experimental spectrum multiple dimensions and Eq. (12) must be used.

In the following sections, different well-known spectroscopic effects are examined from the time-dependent viewpoint. The underlying principles for the different phenomena turn out to be very similar and can be easily rationalized with the theoretical tools presented in this section.

3. SPECTROSCOPIC EXAMPLES

3.1. Intensity Borrowing

In this section we calculate how an absorption transition to an electronic state with a spin different from that of the ground state acquires intensity by spin-orbit coupling with a second state with

the same spin as that of the ground state. The question that we will address is how does a given diabatic potential surface, to which the transition dipole moment from the ground state is zero, acquire intensity? There are many examples in the spectra of transition metal compounds where a spin-forbidden transition is observed in the experimental spectrum because it borrows intensity by spin-orbit coupling with spin-allowed d-d or charge transfer transitions. In the time-domain picture, a forbidden transition means that the initial wavepacket is multiplied by zero (the transition dipole moment) and thus does not have any amplitude on the potential surface of the state with spin multiplicity different from that of the ground state (called "state 1" in this section). However, for the spin-allowed transition the wavepacket is multiplied by the non-zero dipole and the wavepacket is placed vertically from the ground state onto the potential surface (called "state 2"). When spin-orbit coupling is non-zero, amplitude is transferred from state 2 to state 1. It is this transfer of amplitude that causes the observed intensity in the electronic spectrum.

What is the quantitative relationship between amplitude transfer in the time domain and observed intensity in the spectrum in the frequency domain? In order to answer this question we need to examine two aspects of the amplitude transfer: how fast does the amplitude transfer occur, and how much amplitude is transferred? These two aspects are interrelated and depend in part on the coupling strength and the shapes and positions of the potential surfaces. Amplitude transfer occurs immediately after the transition and begins with the first time step in the calculation. Our goal is to calculate quantum mechanically exact spectral intensities and relate them to spin-orbit coupling between the surfaces.

The way in which we follow amplitude transfer between the surfaces is by calculating the populations of the two surfaces as a function of time. The population P_i is defined as the norm of the time dependent wavefunction $\phi_i(t)$:

$$P_i = \langle \phi_i(t) | \phi_i(t) \rangle. \tag{13}$$

At zero time, the population of state 1 is zero and that of state 2 is one.

Model Calculations. In Fig. 2 we present the potential energy surfaces used to calculate intensity borrowing. Excited state diabatic potential surface 1 has a vibrational frequency of 260 cm^{-1}, identical to that of the ground state, but with a potential offset of 0.04 Å along the configurational coordinate Q. The other excited electronic state, diabatic potential 2, has a vibrational frequency of 220 cm^{-1} and its minimum is displaced by 0.25 Å along Q. The energy of the electronic origin transition in Fig. 3 is 11,000 cm^{-1}. These parameters of the potential surfaces were chosen to represent approximately the region of the $^3T_{1g}/^1E_g$ absorption bands in octahedral Ni^{2+} halides with Q representing the totally sym-

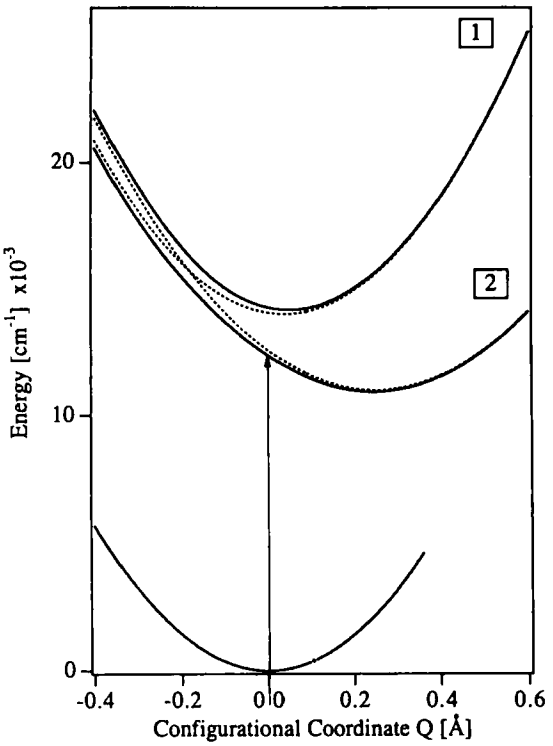

FIGURE 2 Potential energy surfaces for the calculations of intensity borrowing. The adiabatic and diabatic surfaces are shown as bold and dotted lines, respectively. The allowed absorption transition is indicated by an arrow.

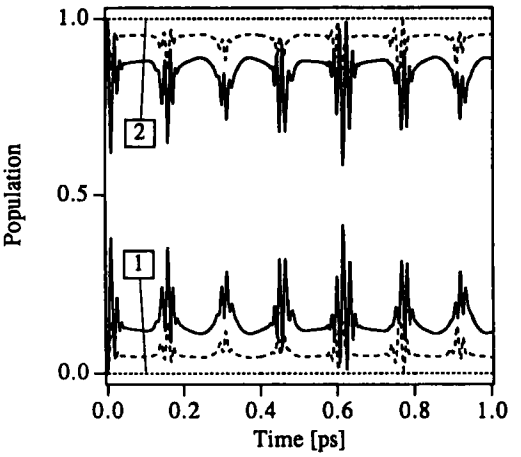

FIGURE 3 Time dependent populations of the diabatic potential surfaces in Fig. 2. Three coupling strengths are shown: V_{12} = 0 cm^{-1} (dotted lines), V_{12} = 300 cm^{-1} (dashed lines) and V_{12} = 600 cm^{-1} (solid lines).

metric breathing mode.[16,17] In these compounds the spin-forbidden band adjacent to a spin-allowed band gains significant intensity.

The norm of the wavefunctions as a function of time is shown in Fig. 3 for three different couplings V_{12}. The transfer of wavepacket amplitude starts at the first time step of the calculation, as outlined in Section 2. Two trends are observed in Fig. 3. First, the "average population" of state 1 becomes higher with increasing coupling. The higher population leads to higher intensity for the transition to state 1 in the absorption spectrum. Second, at times shorter than 50 fs, the transfer of wavepacket amplitude to state 1 increases as the coupling increases. This trend is apparent from the magnitude of the first peak of the population at 20 fs. Therefore the intensity borrowing increases as a function of coupling even in completely unresolved, broadband spectra which are determined by the short-time wavepacket dynamics. It is very easy to qualitatively understand the physical origin of intensity borrowing from the time dependent point of view, in contrast to a time independent approach, where small and often non-obvious changes of the eigenfunctions in the Franck–Condon region need to be calculated.

The calculated absorption spectra for the potential surfaces in Fig. 2 are shown in Fig. 4. All of the calculations are done with

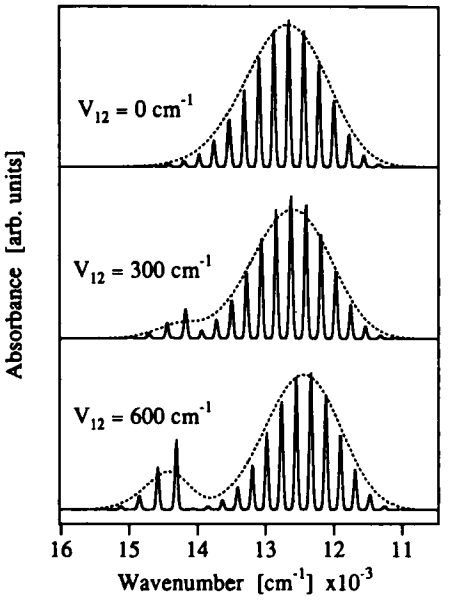

FIGURE 4 Absorption spectra calculated for the potentials in Fig. 2 with damping factors Γ of 15 cm^{-1} (solid lines) and 180 cm^{-1} (dotted lines) at three different coupling strengths.

dipole moments of zero and one for the transitions to states 1 and 2, respectively. In the uncoupled case (V_{12} = 0 cm^{-1}) only the allowed transition is seen in the spectrum. At moderate coupling strength (V_{12} = 300 cm^{-1}) the forbidden transition appears as a shoulder on the high energy side of the allowed transition with enough intensity to be experimentally observable, and it becomes clearly discernible at a coupling strength V_{12} of 600 cm^{-1}. It is easy to numerically determine the ratio of the intensities of the forbidden and allowed absorption bands at every coupling strength. This ratio is plotted in Fig. 5 as a function of V_{12}. It shows a nonlinear intensity increase that can be well described by a second order polynomial. A dependence of the intensity ratio on the square of the spin-orbit coupling parameter is expected from simple perturbation theory,[18] in agreement with our time dependent calculations. The ratios P_1/P_2 of the "average populations" of states 1 and 2 for the three couplings shown in Fig. 3 are included for

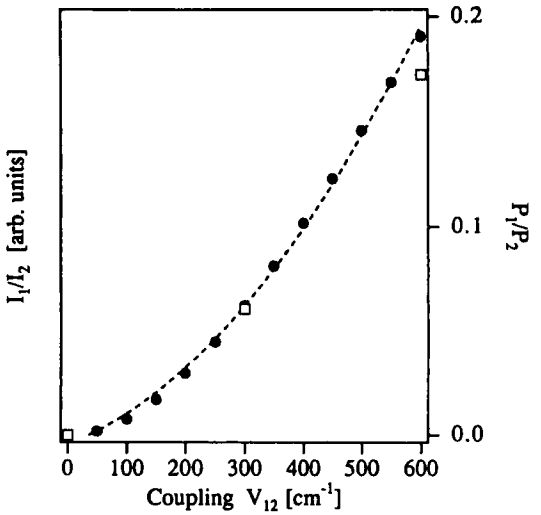

FIGURE 5 Ratio of the intensities of forbidden to allowed bands (Fig. 4) as a function of the coupling strength. Points denote ratios determined from calculated spectra with Γ = 15 cm^{-1}; the dashed curve is a least squares fit to a parabola emphasizing the trend. The ratio of the average populations of states 1 and 2 is given by the open squares at three coupling strengths.

comparison in Fig. 5. The average populations were calculated as the mean values of the populations in the time range shown in Fig. 3. They almost perfectly reproduce the dependence of the spectroscopic intensity ratios on coupling strength, indicating that wavepacket amplitude transfer between states 1 and 2 is indeed the determining factor for intensity borrowing.

The spacing between the vibronic bands in the short progression forming the forbidden absorption band depend on the coupling strength. The effect of coupling on vibronic structure is examined in detail in the next section. At a coupling of 300 cm^{-1} the splitting between the bands of the progression is 261 cm^{-1}, virtually identical to the vibrational energy of diabatic potential 1,260 cm^{-1}. In the bottom spectrum of Fig. 4 the splitting is increased to 275 cm^{-1}, significantly higher than the vibrational energy of the diabatic potential. In the absorption spectra for the Ni^{2+} compounds the same trend is observed: members of the progression forming the ^1E_g band are separated by 300 cm^{-1} in $CsMgCl_3$:Ni^{2+} and $CsNiCl_3$, a splitting that is significantly higher than the ground state a_{1g} frequency (260 cm^{-1}).[16,17] A calculation including the

coupling between the two electronic states is therefore necessary to rationalize the absorption spectra and to determine the correct excited state distortions in these transition metal compounds.

The square of the time dependent wavefunction $\phi(t)$ makes it easy to visualize the intensity borrowing. In Fig. 6 the time dependent wavefunction $\phi(t)$ evolving on the coupled potential surfaces is shown for selected times at a coupling V_{12} of 600 cm^{-1}. At $t = 0$ fs the wavepacket is fully localized on surface 2 and its amplitude on surface 1 is zero. The off-diagonal elements in the Hamiltonian (Eq. (7)) transfer some wavefunction amplitude between the surfaces: at $t = 5$ fs there is some amplitude on state 1, a maximum is reached at about 10 fs and at longer times the shape of the wavefunction on 1 becomes complicated due to the numerous transfers of amplitude between the potential surfaces. This transfer of wavefunction amplitude from state 2 to state 1 affects the autocorrelation function and leads to the induced intensity for the transition to state 1. A very similar situation, leading not to induced intensity but to destructive interferences (antiresonances) in absorption spectra is discussed within the same theoretical model in more detail in Section 3.3.

Summary of Applications to Metal Compound Spectroscopy. It is important to distinguish between different intensity borrowing

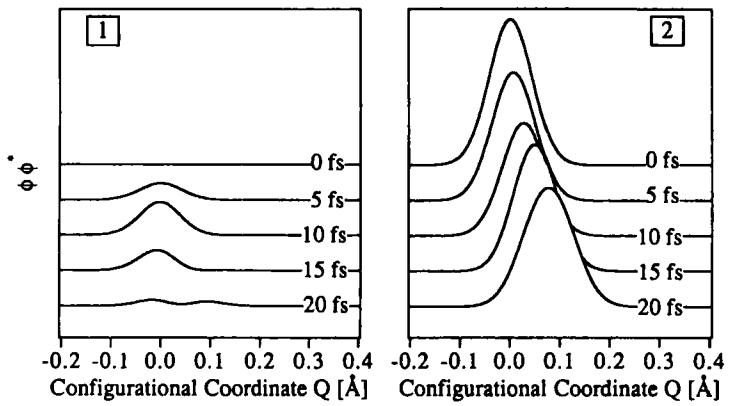

FIGURE 6 The propagating wavefunction $\phi(t)$ at short times in both diabatic states 1 (left hand side) and 2 (right hand side). The coupling V_{12} is 600 cm^{-1}. The traces are displaced along the ordinate for clarity.

mechanisms which are observed in transition metal compounds. In this section an example of "static" (coupling-induced) intensity borrowing was presented. A different intensity mechanism uses ungerade parity enabling modes to give intensity to a band. It leads to absorption spectra with vibronic structure displaced to higher energy by one quantum of the enabling mode. Intensity induced by this mechanism can be calculated with time dependent methods, but obviously multidimensional potential surfaces taking into account all the enabling and totally symmetric modes are needed, leading to situations that are outside the scope of this Comment. A theoretical comparison of the two mechanisms can be found in the literature.[19,20]

From the time-dependent point of view, intensity borrowing between coupled potential surfaces is caused by amplitude transfer. The amplitude transfer is directly related to the strength of the coupling. Other factors not quantitatively discussed in this Comment include the positions of the surfaces, especially the positions of the energy minima. Borrowed intensity increases with the square of the coupling. The time-domain view gives a simple physical picture of the origin of intensity borrowing.

3.2. Vibronic Structure Induced by Coupling

In this section we will focus on the intensity *distributions* (and to a lesser extent on the frequencies) in vibronic progressions in electronic absorption spectra arising from coupled electronic excited states. In the previous section we examined the total (integrated) intensities of electronic bands, whereas here we will examine the individual vibronic components. In the literature, most treatments of the effects of coupling emphasize the electronic part of the wavefunction and the integrated intensities. Our goal is to show how the time-dependent point of view provides both a physical picture and an exact quantum mechanical calculation of the full vibronic part of the problem.

The best-studied and perhaps the most common experimental observations of vibronic structure strongly affected by coupling occur in the absorption and emission spectra of intraconfigurational transitions of metal complexes. The prototypical example is

the lowest energy doublet state of d^3 metal ions in octahedral fields.[21-23] The $^4A_{2g}$ ground state and the ^2E_g excited state both arise from the t_{2g}^3 electron configuration but differ by spin. Because the one-electron transition does not involve a change of orbital population, any bond length changes or force constant changes between the ground and excited electronic state are expected to be very small or zero. Thus most of the vibronic intensity is expected to be found in one line with zero quanta of vibrational excitation (excluding any enabling modes); i.e., no progressions in any of the normal modes would be expected. Frequently, however, short progressions in totally symmetric modes are observed.[22] What causes these progressions?

A second aspect of changed vibronic structure induced by coupling may occur in intensity borrowing. The problem to be addressed in this context is how mixing of two electronic excited states affects the vibronic structure of the two absorption bands involved. Discussions of intensity borrowing, for example by spin-orbit coupling of two states of different spin multiplicity, one of which has a spin-allowed transition from the ground electronic state, usually focus on the electronic wavefunctions. The emphasis is on how much of one electronic wavefunction gets mixed into the second and the resultant effect of the mixing on the oscillator strength of the formerly forbidden transition.[18] Superficially it might be expected that the Franck–Condon factors and hence the vibronic structure would not be affected, an expectation far from the actual result.

General Theoretical Considerations. The interpretation of the effects of electronic state coupling on vibronic structure can artificially be separated into two categories: the effects of the coupling on the "shapes" of the adiabatic potential surfaces, and the effects of the transfer of amplitude between the two diabatic surfaces. This separation is of course impossible and incorrect, but it provides a starting point for defining the effects.

Consider first the "shapes" of the adiabatic surfaces. As a pedagogical starting point, consider two harmonic diabatic surfaces that are coupled. In general, as the coupling between the surfaces increases, the adiabatic surfaces become less and less harmonic. The effective "force constant," or more precisely the curvature at

the minima of the surfaces, will change. In addition, both the position of the minimum and the energy of the minimum will change. Two examples of these effects are shown in Fig. 7. If the two diabatic harmonic surfaces are nested as shown in Fig. 7a, and if the upper surface has a smaller force constant than the lower surface, then the effect of coupling between the two is to broaden the lowest energy adiabatic surface compared to the lowest diabatic surface and sharpen the upper adiabatic surface compared to the upper diabatic surface. For the case of constant nonzero coupling V_{12} as shown in Fig. 7a, the anharmonicity, the force constants and the minimum energies of the potential surfaces change. (The positions of the minima along the coordinate Q remain constant.) Next, consider two harmonic diabatic surfaces, one of which is displaced and the other of which is not displaced from the minimum of the ground state surface along the normal coordinate as shown in Fig. 7b. Again, as the coupling between the surfaces increases, the adiabatic surfaces become less and less harmonic. In this example, the lowest adiabatic surface becomes asymmetric, and most importantly, the position of the minimum shifts along the normal

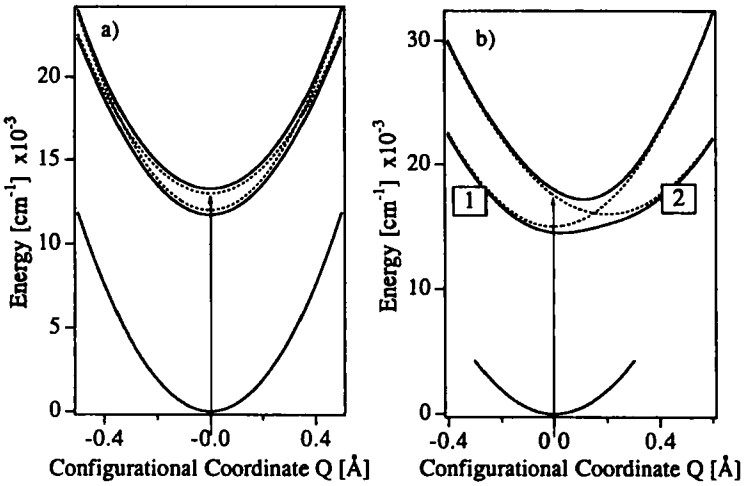

FIGURE 7 Potential energy surfaces illustrating excited state distortions induced by coupling between two electronic states. Adiabatic potentials for a coupling V_{12} of 1200 cm^{-1} are given as solid lines, diabatic potentials as dotted lines. The arrows denote absorption transitions.

coordinate in a direction toward the position of the minimum of the upper diabatic surface. This shift results in a "displacement" of the minimum along the normal coordinate caused by the coupling.

The effect of the above two changes in the vibronic structure in electronic spectra resulting from transitions to or from the undisplaced diabatic surface is qualitatively predictable. The change in the "force constant" and/or the introduction of anharmonicity will cause vibronic intensity to appear in bands which are forbidden in the diabatic picture. Thus the spectrum will change from one line to a vibronic progression in the normal mode corresponding to the coordinate in Fig. 7a. Likewise, the change of the potential minimum along Q in Fig. 7b will also cause a vibronic progression to appear instead of the single band expected without coupling.

Consider next the effects of the transfer of amplitude between the two diabatic surfaces. The most important aspect for this section is the fact that the wavepacket exhibits dynamics on both coupled surfaces and thus the spectra will show vibronic features from both surfaces. Because amplitude is transferred between surfaces and the wavepacket is constantly changing, the vibronic structure in the spectrum will be different from that caused by placing the initial wavepacket at zero time onto one surface only and adding the spectra obtained for both surfaces. Another consequence of the transfer between the two coupled states is the change in the total intensities in the absorption bands from those expected with no coupling and hence no transfer. The total band intensities were discussed in the previous section. Still another important effect is the interference, both constructive and destructive, between the two wavepackets. The unusual spectroscopic features caused by the interference will be the subject of the next section.

A simple starting point for understanding the reasons for vibronic intensity induced by amplitude transfer is to qualitatively note that the wavepacket which develops amplitude on a given surface due to coupling will be far different from a wavepacket $\phi(t = 0)$ which is placed on the surface. From just this qualitative point of view it is to be expected that the autocorrelation functions and hence the spectra will be different. In the example of two coupled surfaces shown in Fig. 7b, let the lower excited state surface represent the lowest doublet excited state of a d^3 metal and

the upper surface represent the lowest quartet excited state. If we assume that the force constant of the ground and doublet excited states are the same and that the transition dipole is non-zero, the initial wavepacket which is placed on the doublet surface is an eigenfunction of the surface and the spectrum in the uncoupled system would consist of one line. However, because the transition to the doublet excited state is spin-forbidden, the electronic transition will place the wavepacket only on the upper surface at $t = 0$. In the coupled system, amplitude will be transferred to the doublet surface and that part of the wavepacket will move on the surface. The transferred wavepacket will contribute to $\langle\phi|\phi(t)\rangle$ and vibronic structure from the doublet surface will appear in the spectrum. The vibronic structure can be quite different from the one-line spectrum. These qualitative considerations should not be pushed too far, but they provide a physical picture that together with the qualitative changes in the adiabatic potentials can help to explain induced vibronic structure.

Model Calculations. The spectra resulting from a transition from a harmonic ground state to the excited state potential surfaces shown in Fig. 7 illustrate the qualitative discussion above. The qualitative discussion was very artificial because it emphasized either the diabatic or the adiabatic parts of the problem rather than the complete problem. The purpose of the model calculations is to provide exact results for the models chosen.

First consider the nested potential surfaces in Fig. 7a. The exact calculations show that this type of situation does not result in much induced vibronic intensity when physically meaningful differences in the force constants of the potentials ($\sim$10%) are used and when the state separation energy (the separation of the minima of the diabatic surfaces) is at least four vibrational quanta. The potentials shown in Fig. 7a have vibrational frequencies of 300 cm^{-1} for the ground state and lower diabatic potential and 270 cm^{-1} for the higher energy diabatic potential. The minima of the diabatic potentials are separated by 1000 cm^{-1}. Very pronounced vibronic intensity changes occur at the energies where the diabatic potential surfaces cross. These effects are treated in the next section. In the case of the undisplaced nested potentials, the crossings can only occur at energies much higher than those of the intense vibronic

transitions unless there are very large differences between the force constants describing the potential and/or the energy separation between the surfaces is on the order of one vibrational quantum. Because these situations are not very common, we will not analyze them further.

The most commonly encountered disposition of potential surfaces is that illustrated by the example in Fig. 7b where the minima are displaced both in energy and in normal coordinate space from each other. The vibrational frequencies of the potentials are identical to those in Fig. 7a. The minimum of the undisplaced diabatic potential is 15,000 cm^{-1} higher in energy than the ground state potential minimum and 1000 cm^{-1} lower than the minimum of the displaced diabatic potential. The distortion along the coordinate Q is 0.2 Å. The absorption spectra resulting from the surfaces defined in Fig. 7b are shown in Fig. 8 as a function of the magnitude of the coupling between the surfaces. The figure shows that the relative intensities of the vibronic features from each individual state change as a function of coupling. The vibronic structure is not simply a progression multiplied by a constant related to the coupling strength. In the "forbidden" state, for example, signifi-

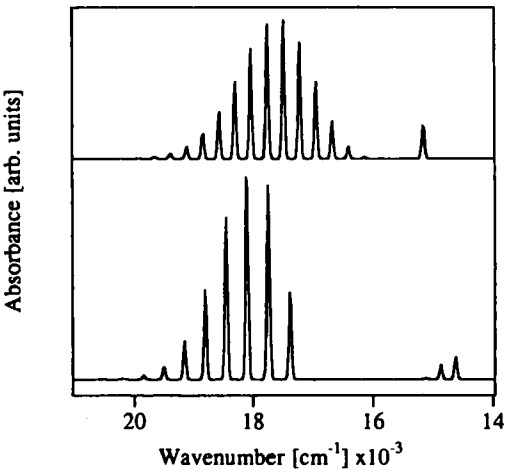

FIGURE 8 Absorption spectra calculated with the potential energy surfaces in Fig. 7b. The coupling constant V_{12} is 0 cm^{-1} and 1200 cm^{-1} for the top and bottom spectra, respectively.

cant intensity appears in the $n = 1$ quantum *even though the diabatic potential surface for this state is undisplaced and there is no force constant change between the ground and excited states.* Likewise, the relative intensities between the vibronic peaks in the allowed transition change as the coupling is changed.

The numerical values of the intensities can readily be calculated by using the split operator method. No simple relationships can be defined. In fact, the trends do not necessarily follow a simple pattern. For instance, in the vibronic peaks of the "forbidden" transition shown in Fig. 8 the ratio of the $n = 1$ to $n = 0$ intensity increases as the coupling is increased from a few wavenumbers to a few hundred wavenumbers and then decreases as the coupling is further increased. The numerical values depend on the "warping" of the potential surfaces and on the amplitude transfer between the surfaces and thus must be calculated on a case by case basis.

Summary of the Applications to Metal Compound Spectroscopy. The electronic spectra of transition metal compounds form a rich area for investigating the effects of potential surface coupling because one of the important sources of state coupling, spin-orbit coupling, is large and because frequently many excited electronic states with different displacements and force constants lie relatively close together in energy. The best investigated cases historically have involved the doublet and quartet states of d^3 metal ions in cubic fields. In highly resolved spectra of these compounds, vibronic progressions are observed on the band from the doublet. The observation is unexpected for an intraconfigurational transition which should not cause a change in force constant nor a change in the potential surface minimum. The above discussion showed how spin-orbit coupling between the doublet and the displaced quartet state can lead to vibronic features in the spectrum.

3.3. Interference Dips in Absorption Spectra

In this section we examine still another spectroscopic manifestation of amplitude transfer between two potential surfaces, interference dips in absorption spectra. In the previous two sections we showed that amplitude transfer can result in changes in the intensities of

electronic transitions and changes in the intensities of individual vibronic components of electronic bands. In the course of our research, we became interested in a little-known but not uncommon phenomenon observed in transition metal spectra, sharp losses of intensity in broad, unresolved bands. We asked ourselves if we could understand and quantitatively calculate these "dips" by using coupled surfaces and amplitude transfer. We found that these rather mysterious dips can be explained in a natural way, and we describe the physical picture and the calculations in this section.

A precedent for dips in intensity in broad bands is found in atomic spectroscopy. Atomic states whose energies lie within a dissociation continuum can give rise to sharp dips in the continuum band. These dips were interpreted by Fano *et al.* and are known as "Fano antiresonances."[24] Fano's equation has been adopted in its entirety to treat the dips arising from molecular states involved in the transition metal spectra, and these molecular spectroscopic features have also been called Fano antiresonances. Examples include complexes of V^{2+}, Cr^{3+}, and Eu^{2+}.[25-28] The antiresonances are unexpected; absorption spectra arising from transitions to two or more nearby electronic states are commonly assumed to be the superposition of the bands arising from transitions to each state individually.

Model Calculations: The model which will be used to illustrate interference effects in absorption spectra is based on the three potential surfaces shown in Fig. 9. The ground state surface is a harmonic potential surface with its minimum at zero along a totally symmetric normal coordinate. The surface is constructed to be representative of the potential along a metal–ligand stretching coordinate. In this example the mass is 16 g/mole and the vibrational frequency is 500 cm^{-1}. The energy (in cm^{-1}) and the displacement (in Å) are shown. The first diabatic excited state potential surface is constructed to be representative of an undisplaced ligand field excited state of a transition metal complex with a vibrational frequency of 500 cm^{-1}. Its minimum is 14,000 cm^{-1} above that of the ground state surface. The second diabatic excited state potential surface represents a ligand field excited state displaced by 0.2 Å along the metal–ligand stretching coordinate. It is constructed to represent an excited state vibrational frequency

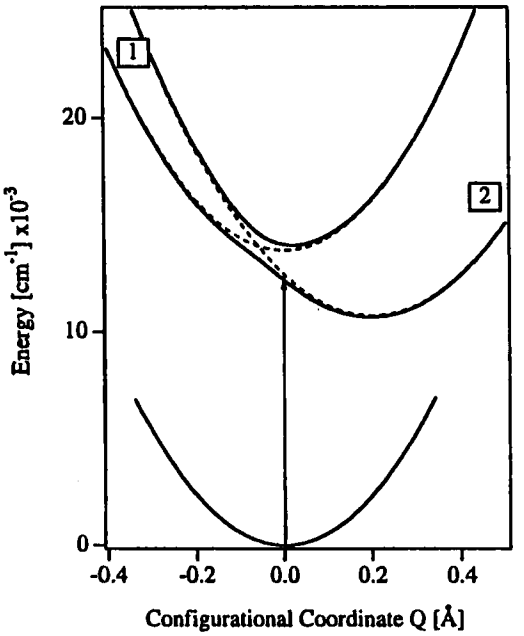

FIGURE 9 Potential energy curves for the absorption transition showing an interference dip. The diabatic potentials for electronic states 1 and 2 are shown by dashed lines, the adiabatic potentials with V_{12} = 600 cm^{-1} are shown by solid lines.

of 450 cm^{-1}. Its lowest energy level is 11,000 cm^{-1} above that of the ground state surface. The two diabatic surfaces cross at an energy of 13,930 cm^{-1} and a value of -0.057 Å along the normal coordinate.

The two excited state surfaces are coupled by spin-orbit coupling. Typical magnitudes of the coupling are 10^2 cm^{-1}. The adiabatic surfaces shown in Fig. 9 illustrate a coupling V_{12} of 600 cm^{-1} (Eq. (6)). The calculations in the following are based on a coupling V_{12} of 300 cm^{-1}; a larger coupling is shown in Fig. 9 in order to more clearly illustrate the avoided crossing.

The calculation of the absorption spectra follows the procedure described in the theory section. For the model illustrated in Fig. 9, the transition dipole moment to diabatic surface 1 (the doublet state) is chosen to be zero for this spin-forbidden transition. Thus the initial wavepacket is placed only on diabatic surface 2, cor-

responding to the spin-allowed quartet–quartet transition in an octahedral d^3 complex.

The electronic absorption spectrum calculated by using the potential surfaces discussed above is shown in Fig. 10a. The spectrum shown by the solid line was calculated with a damping factor Γ of 15 cm^{-1} and shows the individual vibronic peaks. The spectrum shown by the dotted line was calculated with a damping factor of 180 cm^{-1} and shows the envelope of the absorption band. The most important feature of the spectra is the dip in the envelope at about 14,000 cm^{-1}. The more highly resolved spectrum shows that

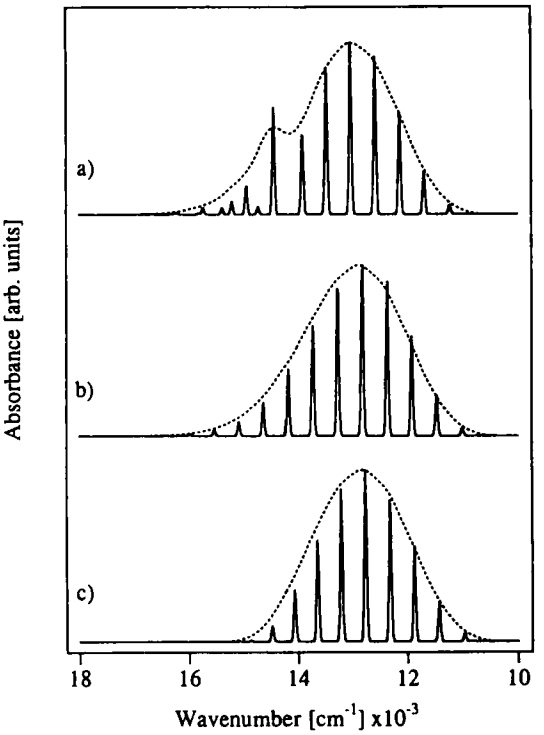

FIGURE 10 Absorption spectra calculated for the potentials shown in Fig. 9 with damping factors Γ = 15 cm^{-1} (solid line) and Γ = 180 cm^{-1} (dashed line). (a) Absorption spectrum with transition moments of 0 and 1 for diabatic states 1 and 2, respectively, and V_{12} = 300 cm^{-1}. (b) Absorption spectrum for uncoupled diabatic potentials (V_{12} = 0 cm^{-1}). (c) Absorption spectrum for a transition to the lower adiabatic surface only.

the dip is caused by a decrease in the intensity of the vibronic feature at 13,900 cm^{-1} and an increase in the intensity of the band at 14,420 cm^{-1}. This dip has been observed in the absorption spectra of d^3 transition metal complexes and has been called a Fano antiresonance. It is a consequence of interference between the two excited electronic states as will be discussed below.

The presence of the interference effect can be most clearly observed by comparing the spectrum calculated from the coupled potential surfaces with that calculated from the uncoupled surfaces shown in Fig. 10b. The spectrum calculated with zero coupling consists of a Poisson distribution of equally spaced vibronic bands originating from the harmonic potential surface 2 (Fig. 9). No bands are observed from surface 1 because the transition dipole is zero.

The dip is caused by the interference between the two electronic states and is not a result of the anharmonic nature of the adiabatic surfaces. The spectrum calculated by propagating the wavepacket on the lowest adiabatic surface is shown in Fig. 10c. This spectrum does not contain the dip in the envelope or the decrease in the intensity of the seventh vibronic band as is observed in the complete spectrum. The spectrum which arises from the two coupled potential surfaces is *not* the sum of the spectra which can be calculated by propagating the wavepacket individually on the two adiabatic surfaces.

Time-Domain Explanation of the Interference. The origins of the dip in the absorption spectrum as well as the other features in the spectrum discussed above can be interpreted by examining the wavepacket in the time domain. First, the $\langle\phi|\phi(t)\rangle$ will be discussed. Second, the individual wavepackets on the two surfaces will be examined. The populations of the two states will also be calculated. Finally, the short-time behavior of the wavepackets and the overlaps will be discussed.

The time dependence of the absolute value of the overlap is shown in Fig. 11a. The dashed line shows the overlap for the case of zero coupling between the surfaces and the solid line shows it for a coupling of 300 cm^{-1}. The damping factor is 15 cm^{-1} in both cases. The difference between the two cases is shown in Fig. 11b. The features which will play an important part in the following

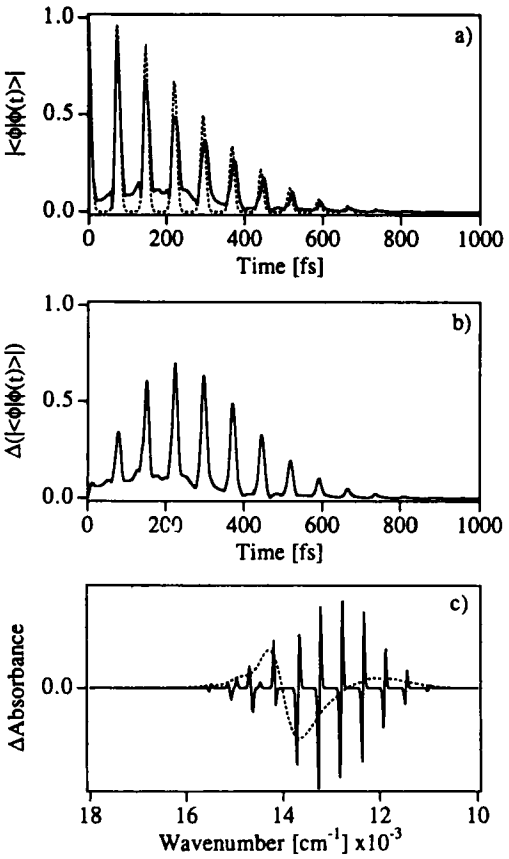

FIGURE 11 (a) Time dependence of the absolute overlap for the absorption transition in Fig. 9 with V_{12} = 300 cm^{-1} (solid line) and V_{12} = 0 cm^{-1} (dashed line). The damping factor Γ is 15 cm^{-1} for both curves. The corresponding absorption spectra are shown in Figs. 10a and 10b, respectively. (b) Absolute difference overlap as a function of time. (c) Difference absorption spectrum resulting from a Fourier transform of the difference overlap (Fig. 11b). The solid and dashed lines are for Γ = 15 cm^{-1} and Γ = 180 cm^{-1}, respectively.

discussions are the faster initial decrease in the overlap, the nonzero overlap between the major recurrences, the smaller magnitude of the recurrences, and the unequal time intervals of the recurrences for the coupled surfaces compared to the uncoupled surfaces. The Fourier transform of the overlap difference is shown

in Fig. 11c. This figure shows the difference between the spectra calculated from the coupled and uncoupled surfaces (Figs. 10a and 10b). Note that for the highly resolved difference spectrum (solid line), each peak consists of a positive and a negative component of unequal magnitude. The positive and negative components of a given peak (the "derivative-like" shape) correspond to the energy shift of the vibronic bands in the coupled vs. the uncoupled spectra. The difference between the magnitudes of the positive and negative components of a given peak correspond to the gain or loss of intensity of that peak. The "envelope" of the difference, calculated by using a damping factor of 180 cm^{-1} (dotted line) clearly shows the region where the interference "dip" in the envelope is observed as well as the region where intensity borrowing results in features associated with the forbidden diabatic state.

The explanation for the difference in the time dependences of the overlaps for the coupled and uncoupled surfaces is obtained by examining the time-dependent wavepacket moving on the coupled surfaces. The wavepacket propagating on surface 2 (Fig. 9) is shown at nine times ranging from zero to 32 fs in Fig. 12a. The figure clearly shows the peak of the wavepacket moving away from the Franck–Condon region toward larger distances under the influence of the non-zero slope of diabatic state 2. Note that the height of the wavepacket rapidly decreases, reaching a minimum at 8 fs. Also note that the wavepacket does not retain a Gaussian form. A significant bump is observed in the region of $Q = 0$ Å at 16 fs and persists at all of the times shown in the figure. The rapid decrease and the bump are a result of population changes between the coupled states. The wavepacket at longer times is shown in Fig. 12b. The return of the wavepacket at one vibrational period of 80 fs is responsible for the first major recurrence in $\langle\phi|\phi(t)\rangle$ shown in Fig. 11. By the second major recurrence at 160 fs the wavepacket has developed a complicated shape with many small peaks and valleys. These new features prevent $\langle\phi|\phi(t)\rangle$ from achieving its initial value of 1.

The time-domain explanation of the interference dip in the absorption spectrum is summarized by examining the short-time overlaps shown in Fig. 13. When the two surfaces are coupled, the total overlap rapidly decreases but does not decrease to zero, as shown by the solid line. In the case of a coupling of 600 cm^{-1}

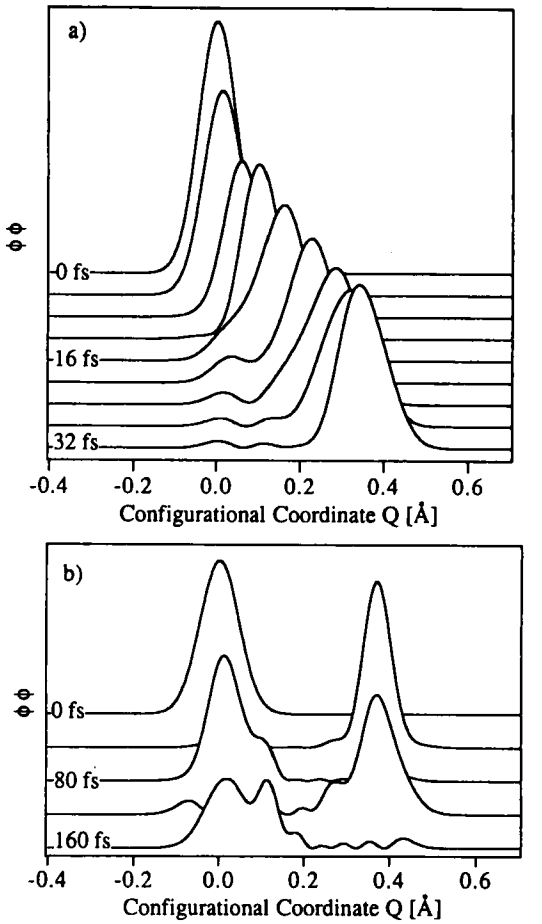

FIGURE 12 The propagating wavefunction ϕ in diabatic potential 2 (Fig. 9) at selected times for a coupling V_{12} = 600 cm^{-1}. The traces are displaced along the ordinate for clarity. (a) Short time development of the initial wavepacket, time increment 4 fs. (b) Longer time dynamics for the same wavepacket, time increment 40 fs.

shown in Fig. 13, the overlap reaches a local minimum at about 10 fs, increases to give a small recurrence at about 13 fs, then slowly decreases. In contrast, the overlap for the uncoupled surfaces decreases smoothly to zero. The initial decrease is less rapid than that calculated with coupling. The more complicated behavior

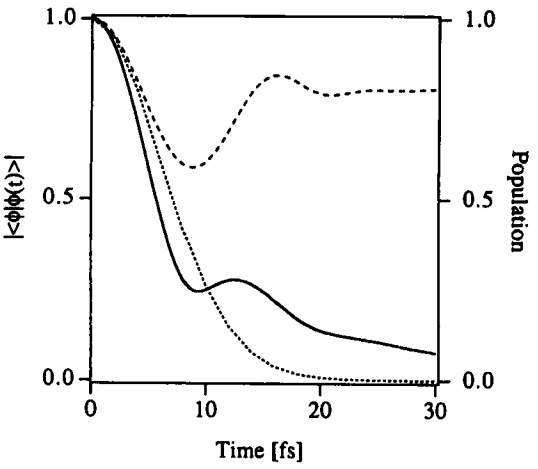

FIGURE 13 The absolute overlap for $V_{12} = 0\ cm^{-1}$ (short dashes) and $V_{12} = 600\ cm^{-1}$ (solid line) at short times ($\Gamma = 15\ cm^{-1}$). The population of state 1 for $V_{12} = 600\ cm^{-1}$ is shown for comparison (long dashes, right-hand ordinate scale).

of the overlap with coupling is explained by the population changes which take place. The population of diabatic surface 2 is shown by the dotted line on the same time scale as the overlaps in Fig. 13. The population is one at $t = 0$ fs, then it decreases rapidly, reaches a local minimum at about 10 fs, and increases to reach a local maximum at about 15 fs. The initial decrease corresponds to loss of population to diabatic surface 1 followed by net back transfer of some population. The overlap roughly follows the population, although its magnitude is not simply proportional to the population because the properties of the wavefunction are changed when the population changes. When compared to the overlap for the uncoupled case, the decrease is more rapid at short time but a recurrence is also observed. When transformed to the frequency domain, the more rapid decrease results in a broader spectrum, i.e., in more intensity at higher energies and less intensity at lower energies in the spectrum relative to that in the uncoupled case. The small recurrence at about 13 fs corresponds to a separation between bands in the frequency domain of $c^{-1}t^{-1}_{\text{recurrence}} = 2600\ cm^{-1}$. The net result of these two effects is to produce a spectrum for the coupled case in which an interference dip is observed in

the envelope as shown in the spectrum in Fig. 10a and in the difference spectrum in Fig. 11c. Again, it is easily rationalized from the calculations in the time domain.

Summary of Applications to Metal Compound Spectroscopy. Interference effects, large or small, always occur between two potential surfaces when the surfaces are coupled. Many other potential surfaces were examined; the results show that interference effects exist, but may not always be as prominent as those discussed here. The model which we presented was chosen in order to represent known spectroscopic examples where clearly discernible dips in the absorption band envelopes are observed. We have applied our model to a coordination compound of chromium(III).[29]

Interference dips are prize examples of cases where calculations and interpretation in the time domain are very powerful. If we were to limit ourselves to the clamped nuclei picture where the energy levels are rungs on a ladder, then the total spectrum would be the sum of the spectra caused by transitions to each of the individual rungs and dips in the total spectrum would not occur. In the time domain, many types of intensity effects including borrowing, vibronic structure and dips can be understood.

3.4. Excited State Jahn–Teller Distortions

We now turn our attention to the Jahn–Teller problem, a situation where nuclear motion is a necessary part of the physical problem. It would be incorrect to treat the spectrum of a molecule with a Jahn–Teller active excited state in terms of clamped nuclei. If the nuclei could be clamped into the positions they occupy in the ground electronic state, an excited state could be degenerate. However, Jahn and Teller showed that for every point group, a nonlinear molecule will have a normal mode of vibration which prohibits the degeneracy from existing.[2] Thus both the electronic and the nuclear parts of the wavefunction must be considered simultaneously and Born–Oppenheimer separability cannot be assumed.

We can treat the Jahn–Teller problem exactly by using the techniques that we have been discussing. The potential surfaces that we will use are shown in Fig. 14. The surfaces are similar to those

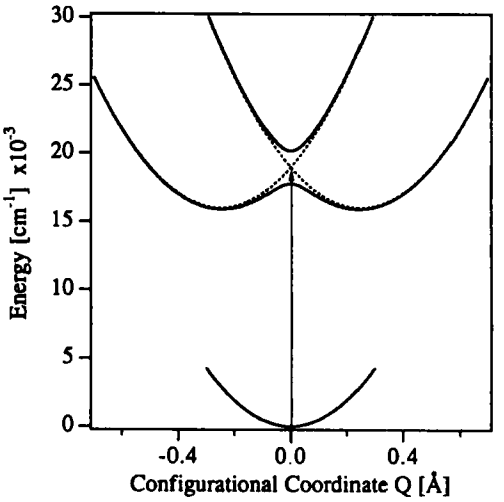

FIGURE 14 Potential energy surfaces for a $E_g \times b_{1g}$ Jahn–Teller effect. The adiabatic excited state potentials for a coupling V_{12} of 1200 cm^{-1} are shown as bold lines. The diabatic excited state potential surfaces are shown as dotted lines.

that we have been using in the previous sections. However, there are three important differences. First, the surfaces are symmetric about the origin, i.e., the minima of the diabatic surfaces have the same energy, are located at $\Delta Q_1 = -\Delta Q_2$ and cross at $Q = 0$ Å. Second, the wavepacket is placed on both of the diabatic surfaces with equal amplitude. Thus there will not be net amplitude transfer between the surfaces. Third, the coordinate Q is a non-totally symmetric normal coordinate and is known as the "Jahn–Teller active" mode. Because we are considering only one dimension in this Comment, the relevant physical problem corresponds to the b_{1g} non-totally symmetric mode (one-dimensional) and an E_g excited state in the D_{4h} point group.

A large number of comprehensive theoretical treatments of the Jahn–Teller effect exist[30,31] and the spectroscopic manifestations have been discussed.[23,32] It is our goal to demonstrate that time dependent calculations provide an easy way to calculate electronic spectra involving the Jahn–Teller effect and to determine excited state distortions along the Jahn–Teller active vibrational modes. A large advantage of time dependent computational techniques is

that no a priori distinction between static or dynamic Jahn–Teller situations needs to be made; the computational scheme handles these limiting situations as well as all intermediate cases exactly.

Model Calculations. The potential surfaces for a one dimensional Jahn–Teller situation in the lowest energy excited state are shown in Fig. 14. The excited state has two components and the diabatic potential surfaces cross at $Q = 0$ Å, the ground state equilibrium geometry. The vibrational frequency for the ground state and the two diabatic excited state surfaces is 300 cm^{-1} and the excited state potential minima are located at ± 0.25 Å along the configurational coordinate. The energy of the electronic origin transition E_0 is 16,000 cm^{-1}.

The absorption spectra calculated from the potential surfaces in Fig. 14 at various coupling strengths are shown in Fig. 15. At zero coupling (Fig. 15a) a Poisson-shaped absorption band is observed, identical to the spectrum calculated for a nondegenerate excited state with its potential identical to one of the diabatic potentials of the degenerate state. The long progression with a spacing of 300 cm^{-1} indicates that the molecule is distorted along Q in the excited state. With increasing coupling the bandshape becomes more and more different from a Poisson distribution and the vibronic splittings change.

The overall bandshapes, shown by dotted lines in Fig. 15, show a very distinct dependence on coupling strength. The Poisson bandshape at zero coupling in Fig. 15a changes into a double maximum band for the weakly coupled situation in Fig. 15b (V_{12} = 150 cm^{-1}). This bandshape with maxima at 18,500 cm^{-1} and 19,800 cm^{-1} is reminiscent of unresolved absorption bands observed in a variety of Ti^{3+} doped lattices.[23,33] The high energy component of the broad double maximum band becomes more and more intense with increasing coupling. The spectra with coupling strengths of 400 cm^{-1} and 1200 cm^{-1} illustrate this trend and are shown in Figs. 15c and 15d, respectively. With increasing coupling strength the adiabatic potential surfaces at $Q = 0$ Å become more and more separated in energy and the upper potential looks more and more similar to the ground state potential energy surface, thus favoring transitions to levels of the coupled states with energies near the bottom of the upper adiabatic potential surface. At the

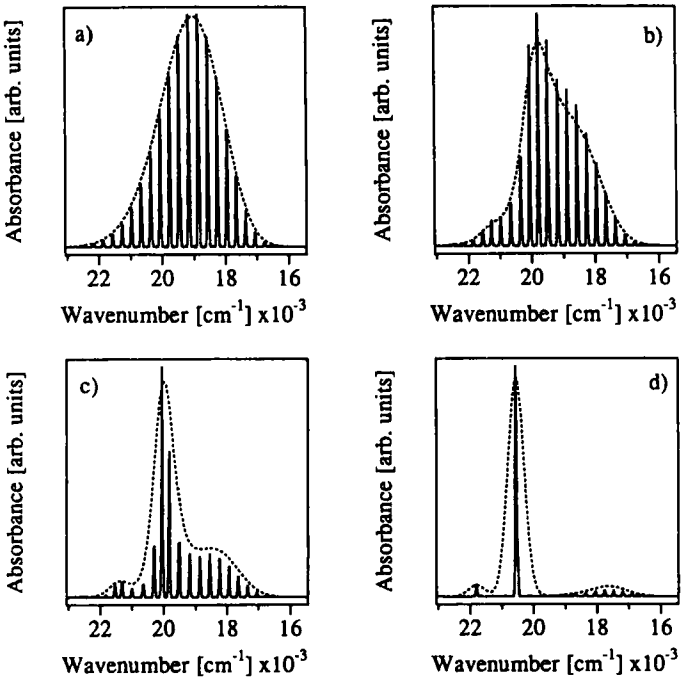

FIGURE 15 Calculated absorption spectra for the potential surfaces of Fig. 14. The solid and dotted spectra are calculated with Γ = 15 cm^{-1} and 180 cm^{-1}, respectively. The coupling matrix elements V_{12} are (a) 0 cm^{-1}, (b) 150 cm^{-1}, (c) 400 cm^{-1}, (d) 1200 cm^{-1}.

highest coupling strength, shown in Fig. 15d, the spectrum is dominated by a single sharp line, corresponding to the dynamic Jahn–Teller effect.

The absolute autocorrelation functions for the potentials in Fig. 14 as a function of the coupling strengths provide a satisfying explanation of the spectra changes in Fig. 15. The autocorrelation is shown in Fig. 16 for different coupling strengths. At zero coupling the time dependence of the absolute overlap is exactly identical to that for a displaced nondegenerate excited state, with recurrences at 110 fs corresponding to the splitting of 300 cm^{-1} of the progression in Fig. 15a. The time dependence of the overlap becomes very complicated with increasing coupling, reflecting the dynamics of the wavepacket on the coupled surfaces. For a cou-

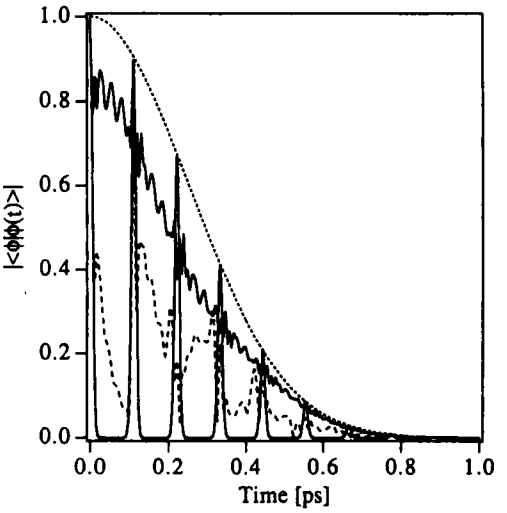

FIGURE 16 Time dependence of the absolute overlap for the wavepacket propagating on the surfaces in Fig. 14 with V_{12} = 0 cm^{-1} (solid line), V_{12} = 400 cm^{-1} (dashed line) and V_{12} = 1200 cm^{-1} (bold line). The overlap for a wavepacket on a nondisplaced, nondegenerate harmonic potential is shown by the dotted line.

pling V_{12} of 400 cm^{-1} the dominant recurrences are still at 110 fs, and consequently the main progression observed in the calculated spectrum (Fig. 15c) has a splitting near 300 cm^{-1}. An interesting trend in the time dependence of the absolute overlap is observed as the coupling gets stronger: the "gaps" between the main recurrences of $|\langle\phi|\phi(t)\rangle|$ are more and more "filled in" leading to an autocorrelation function reminiscent of the time dependent overlap for an undisplaced excited state, indicated by the dotted line in Fig. 16. The overlap for a coupling V_{12} of 1200 cm^{-1} still shows recurrences at 110 fs, coinciding with the main recurrences for the weaker couplings, but prominent recurrences separated by approximately 24 fs are also observed. They correspond to an energy of 1390 cm^{-1}, which is easily discernible in the spectrum shown in Fig. 15d as the difference between the most intense transition at 20,510 cm^{-1} and the transition at 21,840 cm^{-1}. The final states of these transitions can be visualized as states on the higher energy adiabatic potential energy surface with its minimum at zero displacement along Q, leading to a spectrum as expected for an un-

distorted molecule. This picture is intuitively helpful, but quantitatively wrong: the total spectra calculated for all the coupled potential surfaces in this Comment are *not* equal to the sum of the spectra for the individual adiabatic surfaces. It is preferable to look at the autocorrelation function because it provides a clear and quantitatively correct illustration of the transition from the static to the dynamic Jahn–Teller effect.

Potential Application to Metal Compound Spectroscopy. The one dimensional potential surfaces investigated in this section illustrate the power of time dependent computational techniques applied to the Jahn–Teller effect. A one dimensional model is a good starting point for understanding the overall features of broad, unresolved absorption spectra of transition metal complexes, as often observed in compounds of Ti^{3+} and Fe^{2+}.[23,33] The one dimensional model is not sufficient to calculate the resolved vibronic splitting patterns observed in some transition metal complexes with e or t Jahn–Teller active modes because two or three dimensions are needed.[32,34,35] Multidimensional potential surfaces corresponding to the correct electronic and vibrational degeneracies need to be used with the propagation techniques presented in Section 2. For these situations, the coupling between electronic states in multiple dimensions requires calculations with multidimensional potential surfaces. The approximation presented in Eq. (12) is no longer applicable. Time dependent calculations on such multidimensional potential surfaces are very promising for the exact calculation of structured spectra resulting from the well known $E \times e$, $T \times e$ or $T \times t$ Jahn–Teller effects in octahedral complexes.

3.5 Intervalence Electron Transfer Spectra

An interesting class of transition metal complexes that can easily be treated by using the theoretical methods discussed in this Comment is the class of mixed valence complexes.[36] These complexes were surveyed by Robin and Day who proposed a classification scheme which has been widely adopted.[37] The best known of the mixed valence complexes is probably the "Creutz–Taube" complex, $[(NH_3)_4Ru(pyrazine)Ru(NH_3)_4]^{5+}$, which contains two bridged metal ions in two different oxidation states (+2 and +3) with the

same ligands.[38] The mixed valence complex has a low energy transition in the near IR region of the absorption spectrum that is absent when the two metal centers have the same oxidation states (+2 and +2 or +3 and +3). This "intervalence band" results from transitions within a vibronic manifold arising from coupling of the constituent ions.

The theoretical treatment of the intervalence band is a special case of the general picture developed in this Comment because the potential is symmetric and because the spectrum is calculated by propagating the two components of the lowest energy eigenfunctions of the coupled system. The appropriate potential surfaces are shown in Fig. 17. The usual and most simplistic explanation of the intervalence band is based on the diabatic surfaces. In this picture the intervalence band arises from a transition from one diabatic surface to the other (which crudely represents a one-electron transition from Ru(II) to Ru(III)). A second explanation is based on the adiabatic surfaces and visualizes the transition as occurring from the lowest adiabatic surface to the upper adiabatic surface. These two explanations may have some approximate validity in certain limits of the coupling, but they are neither general nor completely correct.

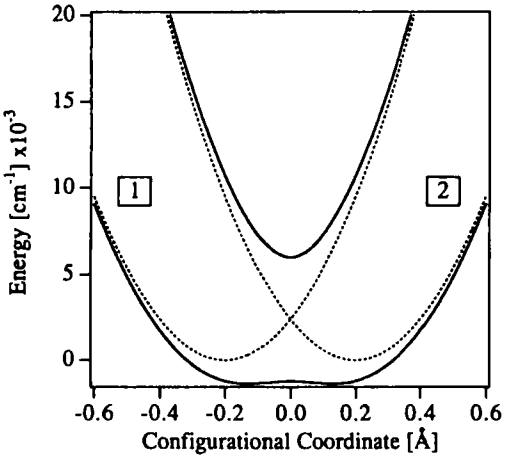

FIGURE 17 Adiabatic and diabatic potential surfaces for a model mixed-valence system.

The complete one-dimensional picture requires that the lowest energy eigenfunction of the coupled surfaces be calculated. This eigenfunction has two components, one from each of the diabatic surfaces. The component from surface one multiplied by the transition dipole is the initial wavepacket that is propagated on surface two, and vice versa. The situation is similar to the Jahn–Teller example discussed above in terms of the breakdown of the Born–Oppenheimer separability of the electronic and vibrational parts of the problem. The major difference is that the initial wavepacket involves the lowest eigenfunctions of the coupled system and not the vibrational wavefunction times the transition dipole from a completely different electronic surface.

The configurational coordinate in Fig. 17 requires further explanation. It is rarely defined precisely, in part because there are usually several possibilities and it is difficult to choose the most important one. In the case of the Creutz–Taube complex some of the limiting choices are motion of the bridging ligand B, i.e., Ru^{+2}–B-Ru^{+3} ↔ Ru^{+3}-B–Ru^{+2}, motion of the cis and or the trans ammonia ligands, i.e., N–Ru^{+2}-B-Ru^{+3}-N ↔ N-Ru^{+3}-B-Ru^{+2}–N, or some combination of these. The coordinate which is chosen here for illustration purposes only is the Ru-N stretching mode which has a vibrational energy around 500 cm^{-1} in many coordination compounds of ruthenium.

Model Calculations. The adiabatic and diabatic potential surfaces representing a one-dimensional model for a mixed-valence compound are shown in Fig. 17. They are chosen to roughly represent the "Creutz–Taube" compound, but we do not attempt a quantitative fit to the absorption spectrum of this compound. The diabatic potentials have a vibrational energy of 500 cm^{-1} and their minima are at ±0.2 Å along the coordinate Q. The coupling constant V_{12} used in Fig. 17 and all of the following calculations is 3600 cm^{-1}. The first step towards calculating the intervalence absorption band is calculating the lowest energy eigenfunctions of the coupled states shown in Fig. 17. Time dependent methods are efficient for finding both eigenvalues and eigenfunctions of a given set of potentials. The theoretical and computational aspects of

these calculations are discussed in the literature.[12,13] The eigenfunctions are calculated as follows:

$$\Psi_i(E_i) = \int_0^T \phi(t)w(t) \exp\left(\frac{iE_i}{\hbar} t\right) dt. \tag{14}$$

Ψ_i denotes the eigenfunction corresponding to the eigenvalue E_i, $\phi(t)$ is the time dependent (propagating) wavefunction and $w(t)$ is a Hanning window function. For coupled potentials, each eigenfunction Ψ_i is an array with two components corresponding to the two diabatic potentials which form the basis in all our calculations. The two lowest energy eigenfunctions of the potentials in Fig. 17 are shown in Fig. 18. The two components of each of the eigenfunctions are shown. It is interesting to note that there is a phase relationship between the two components of each wavefunction; for example they always have opposite signs for the lowest energy level, the lower set of curves in Fig. 18. The eigenvalues of the lowest vibronic levels are 109 cm^{-1}, 191 cm^{-1}, 404 cm^{-1}, and 617 cm^{-1}, with the lower adiabatic potential minima at 0 cm^{-1}. The barrier height of the lower adiabatic surface is 138 cm^{-1}, almost

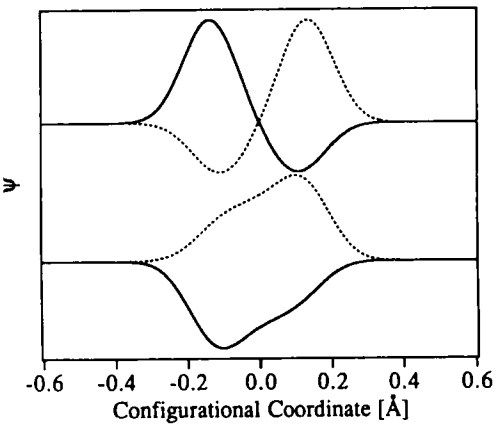

FIGURE 18 The two lowest energy eigenfunctions of the coupled states in Fig. 17. The higher energy eigenfunction is offset along the ordinate for clarity. The two components of each eigenfunction are shown as solid and dotted lines, respectively.

coincident with the lowest energy vibronic level. This low barrier leads to a probability distribution, calculated as the sum of the squared components of the lowest energy eigenfunction, which has considerable probability at $Q = 0$ Å, indicating a strongly delocalized system. In fact, the "Creutz–Taube" compound is found to be strongly delocalized (class III in the scheme of Robin and Day) by a variety of spectroscopic techniques.[39]

The intervalence absorption band at low temperature is easily calculated by using the eigenfunction of the lowest energy level. The transition promotes diabatic state 1's component onto surface 2, state 2's component onto surface 1. This graphically intuitive description should not give the impression that we are resorting to one of the simple models mentioned in the previous paragraph; it is only the most convenient way to express the intervalence transition in our (diabatic) basis. The spectrum is calculated exactly (to the numerical precision of Eq. (9)), as opposed to the majority of time independent methods, where the effects of coupling and therefore the spectra are approximated.[40]

The intervalence absorption band obtained in the low temperature limit is shown in Fig. 19 (solid line). The overall bandshape is very close to a Poisson distribution for small distortions.

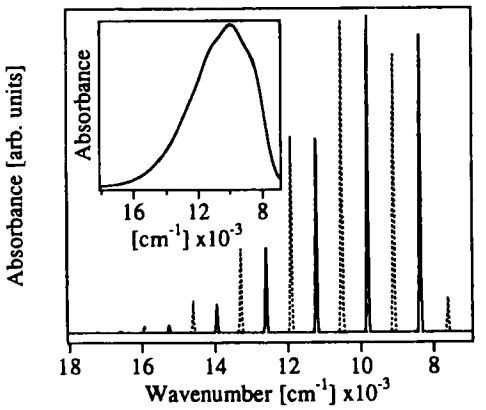

FIGURE 19 Calculated intervalence absorption band ($\Gamma = 15$ cm^{-1}). The solid line spectrum was calculated with the lowest energy eigenfunction, the dotted spectrum with the higher energy eigenfunction shown in Fig. 18. The inset shows the calculated intervalence absorption band at 300 K with $\Gamma = 420$ cm^{-1}.

At nonzero temperatures, higher vibronic levels are thermally populated and can act as initial states for an intervalence transition. At 300 K the populations of the four lowest energy levels in our model system are 50%, 34%, 12% and 4% in order of increasing energy. The calculation of the spectrum therefore consists of four propagations analogous to the one described for the lowest energy eigenfunction. The four spectra are then multiplied by their thermal weights and added to give the total spectrum. In Fig. 19 we show the spectrum obtained for a transition originating from the vibronic level at 191 cm^{-1} (upper eigenfunction in Fig. 18) as a dashed line. This bandshape is distinctly different from a Poisson distribution. Due to the symmetries of the eigenfunctions in the symmetric potentials of Fig. 17, only every other final state of the coupled system has intensity in the intervalence absorption band at $T = 0$ K. The inset to Fig. 19 shows the calculated absorption band at 300 K obtained with the thermal weights at the beginning of this section. The damping factor Γ is 420 cm^{-1}, leading to an almost unresolved spectrum typical for mixed valence compounds. The shape is different from a simple Poisson distribution. In general, intervalence absorption bands can not even approximately be analyzed in terms of a simple harmonic model.

In addition to the intervalence band shown in Fig. 19, the calculated spectrum contains transitions at very low energies, corresponding to transitions between the lowest three vibronic levels. These transitions are hard to measure experimentally because the infrared spectra of coordination compounds at these low energies are dominated by very intense molecular modes not associated with the intervalence electron transfer. We therefore will not discuss these transitions further.

Potential Applications to Metal Compound Spectroscopy. The computational method is not limited to the symmetric situation presented in this example. Models for mixed valence compounds with unequal force constants and minimum positions along the Q and energy axes can be treated with the same high accuracy. A fit to the experimental absorption spectrum therefore leads to quantitative potential surfaces and coupling strength for a mixed valence system. The information resulting from a fit can be used to classify any molecule in the scheme of Robin and Day, but it provides

additional quantitative information. This makes the time dependent approach very attractive for the detailed analysis of a wide variety of intervalence absorption spectra known for transition metal compounds.

4. SUMMARY

In this Comment we have shown how to calculate and interpret spectra from molecules in which the Born–Oppenheimer separation of nuclear and electronic wavefunctions is not valid because of potential surface coupling. We have analyzed some very overt cases, such as Jahn–Teller coupled excited states and intervalence electron transfer spectra. The exact quantum mechanical results showed what spectral features can be expected from these systems. In another overt case, that of interference dips in broad envelopes, we not only provided exact quantum mechanical results but also showed the physical origin of the otherwise mysterious phenomenon. We have also analyzed more subtle cases of unusual spectroscopic features. We examined some details of the relative intensities of vibronic bands. We showed, for example, how vibronic progressions arise in intraconfigurational d-d transitions where no molecular geometry changes are expected in the excited state. We also provided new insight into intensity borrowing in terms of amplitude transfer between surfaces. It is important to note that all of these apparently disparate spectroscopic features were understood by using two coupled surfaces along a non-degenerate normal coordinate.

In our Comment we have emphasized the insight obtained from the time-dependent point of view. We have defined and identified interesting problems. We have illustrated our discussions with exact quantum mechanical calculations. The methods and the new insight are ready to be applied to specific spectra. These methods are not limited to absorption spectra; they are also applicable to emission spectra and resonance Raman excitation profiles. In addition, they can be expanded to multiple dimensions. In future work, specific spectra will be fit by using these techniques in order to determine specific molecular properties of new and interesting molecules.

Acknowledgments

We thank Dr. Eric Simoni, Dr. Jürgen Gauss and Prof. E. J. Heller for helpful discussions. This work was made possible by a grant from the National Science Foundation (CHE91-06471).

References

1. J. I. Zink and K.-S. Kim Shin, *Adv. in Photochemistry*, eds. D. H. Volman, G. S. Hammond and D. C. Neckers, Vol. 16, p. 119 (Wiley, New York, 1991).
2. M. Born and J. R. Oppenheimer, Ann. Physik **84**, 457 (1927).
3. H. A. Jahn and E. Teller, Proc. R. Soc. London, Ser. A **161**, 220 (1937).
4. E. J. Heller, J. Chem. Phys. **62**, 1544 (1975) and J. Chem. Phys. **68**, 3891 (1978).
5. E. J. Heller, Acc. Chem. Res. **14**, 368 (1981).
6. J. Alvarellos and H. Metiu, J. Chem. Phys. **88**, 4957 (1988).
7. X. P. Jiang, R. Heather and H. Metiu, J. Chem. Phys. **90**, 2555 (1989).
8. R. Heather and H. Metiu, J. Chem. Phys. **90**, 6903 (1989).
9. J. Zhang, E. J. Heller, D. Huber, D. G. Imre and D. Tannor, J. Chem. Phys. **89**, 3602 (1988).
10. S. Das and D. J. Tannor, J. Chem. Phys. **91**, 2324 (1989).
11. J. Zhang, E. J. Heller, D. Huber and D. G. Imre, J. Phys. Chem. **95**, 6129 (1991).
12. M. D. Feit, J. A. Fleck and A. Steiger, J. Comp. Phys. **47**, 412 (1982).
13. D. Kosloff and R. Kosloff, J. Comp. Phys. **52**, 35 (1983).
14. For an introductory overview see J. J. Tanner, J. Chem. Ed. **67**, 917 (1990).
15. W. H. Press, B. P. Flannery, S. A. Teukolsky and W. T. Vetterling, *Numerical Recipes* (Cambridge University Press, New York, 1986).
16. G. L. McPherson and G. D. Stucky, J. Chem. Phys. **37**, 3780 (1972).
17. J. Ackerman, E. M. Holt and S. L. Holt, J. Sol. Stat. Chem. **9**, 279 (1974).
18. C. K. Jørgensen, Acta Chem. Scand. **9**, 1362 (1955).
19. G. Orlandi and W. Siebrand, J. Chem. Phys. **58**, 4513 (1973).
20. C. J. Ballhausen and A. E. Hansen, Ann. Rev. Phys. Chem. **23**, 15 (1972).
21. A. D. Kirk, Coord. Chem. Rev. **39**, 225 (1981) and references therein.
22. C. D. Flint and A. P. Matthews, Inorg. Chem. **14**, 1008 (1975).
23. J. Ferguson, Progr. Inorg. Chem. **12**, 159 (1970).
24. U. Fano, Phys. Rev. **124**, 1866 (1961).
25. M. D. Sturge, H. J. Guggenheim and M. H. L. Pryce, Phys. Rev. B **2**, 2459 (1970).
26. A. Lempicki, L. Andrews, S. J. Nettel, B. C. McCollum and E. I. Solomon, Phys. Rev. Lett. **44**, 1234 (1980).
27. A. Meijerink and G. Blasse, Phys. Rev. B **40**, 7288 (1989).
28. H. Riesen and H. U. Güdel, Mol. Phys. **60**, 1221 (1987).
29. C. Reber and J. I. Zink, J. Chem. Phys. **96**, 2681 (1992).
30. I. B. Bersuker, *The Jahn–Teller Effect and Vibronic Interactions in Modern Chemistry* (Plenum Press, New York, 1984).
31. *The Jahn–Teller Effect in Molecules and Crystals*, ed. R. Englman (Wiley-Interscience, London, 1972).

32. M. D. Sturge, Sol. State Phys. **20**, 91 (1967).
33. R. L. Carlin and I. M. Walker, J. Chem. Phys. **46**, 3931 (1967).
34. H. U. Güdel and T. R. Snellgrove, Inorg. Chem. **17**, 1617 (1978).
35. R. B. Wilson and E. I. Solomon, J. Am. Chem. Soc. **102**, 4085 (1980).
36. *Mixed Valence Compounds*, ed. D. B. Brown (Reidel, Dordrecht, 1980).
37. M. B. Robin and P. Day, Adv. Inorg. and Radiochemistry **10**, 247 (1967).
38. C. Creutz and H. Taube, J. Am. Chem. Soc. **91**, 3988 (1969).
39. U. Fürholz, H. B. Bürgi, F. E. Wagner, A. Stebler, J. H. Ammeter, E. Krausz, R. J. H. Clark, M. J. Stead and A. Ludi, J. Am. Chem. Soc. **106**, 121 (1984).
40. S. B. Piepho, E. R. Krausz and P. N. Schatz, J. Am. Chem. Soc. **100**, 2996 (1978).